

Langmuir-like model of dilute impurities in concentrated solid solutions

Jacob Jeffries^{1, 2} and Enrique Martinez^{1, 3}

¹Department of Materials Science and Engineering, Clemson University, Clemson, SC 29634, USA

²Theoretical Division, Los Alamos National Laboratory, Los Alamos, NM 87545, USA

³Department of Mechanical Engineering, Clemson University, Clemson, SC 29634, USA

February 11, 2024

Abstract

High-entropy alloys have drawn recent interest for their promising mechanical properties and irradiation resistance. Various properties, namely transport properties, are controlled by point defect concentration, which must be known before performing atomistic simulations to compute transport coefficients. In this work, we present a general Langmuir-like model for impurity concentration in an arbitrarily complex solid solution and apply this model to generate expressions for concentrations of vacancies and small interstitial atoms. We then calculate the vacancy concentration as a function of temperature in the equiatomic CoNiCrFeMn and FeAl alloys with modified embedded-atom-method potentials for various chemical orderings, showing there is no clear correlation between vacancy thermodynamics and chemical ordering in the CoNiCrFeMn alloy but clear systematic patterns for FeAl.

1 Introduction

High-entropy alloys (HEAs) have recently attracted interest due to their complex design spaces. In particular, the Cantor alloy (equiatomic CoNiCrFeMn) has shown promising mechanical properties^[1] and irradiation resistance^[2]. However, modeling HEAs is not trivial due to their inherent complexities, including large variances in local chemistry, complex thermodynamic behavior, characterization of microstructure, and more. Further complicating the modeling, these individual features can strongly interact with one another. For example, Otto et al. observed the precipitation of a Cr-rich σ -phase at 700 °C and L1₀-NiMn, B2-FeCo, and bcc Cr phases at 500 °C^[3], and Li et al. showed that this phase decomposition is driven by NiMn segregation at grain boundaries^[4].

Additionally, the properties of concentrated alloys can be significantly changed by the presence of dilute substitutional and interstitial impurities. For example, in austenitic stainless steels, Muramaki et al. showed that the concentration of octahedral H significantly affects loading damage and fatigue crack growth rate^[5], Morgan et al. correlated long-term

³H exposure to decreased fracture toughness^[6], and Miura et al. observed a decreased fracture stress of grain boundary brittle fracture from increased He content^[7]. Diffusion in metals is also mediated by substitutional point defects (PDs), and therefore diffusion-controlled properties of alloys strongly depend on PD concentration. In particular, irradiation of alloys increases defect concentration, which is of interest due to the potential application of concentrated alloys in irradiated environments, such as austenitic stainless steels in pressurized water reactors^[8]. Then, in the presence of a PD sink, preferential transport of particular species leads to solute segregation, coined radiation-induced segregation (RIS), which is typically modeled using linear response theory^{[9][10]}:

$$\mathbf{J}_\alpha = - \sum_{\alpha'} L_{\alpha\alpha'} \nabla \mu_{\alpha'} \quad (1)$$

where \mathbf{J}_α is the flux of species α , $\mu_{\alpha'}$ is the chemical potential of species α' , and $L_{\alpha\alpha'}$ is the *equilibrium* α - α' Onsager coefficient, which is a transport coefficient coupling species α and α' .

$L_{\alpha\alpha'}$ is usually estimated by inserting one PD in a

periodic box, simulating transport using an atomistic method such as molecular dynamics^[11] or atomistic kinetic Monte Carlo methods^{[12][13][14]} and evaluating the generalized Einstein relation^[15]:

$$L_{\alpha\alpha'}^{(1)} = \frac{1}{Vk_B T} \lim_{t \rightarrow \infty} \frac{\langle \mathbf{R}_\alpha^{(1)}(t) \cdot \mathbf{R}_{\alpha'}^{(1)}(t) \rangle}{6t} \quad (2)$$

where V is the volume of the box, k_B is the Boltzmann constant, T is temperature, $\mathbf{R}_\alpha^{(1)}(t)$ is the total displacement of α at time t mediated by one PD, and $L_{\alpha\alpha'}^{(1)}$ is the α - α' transport coefficient mediated by one PD. The use of such computationally expensive techniques introduces a system size constraint, though, which results in a PD concentration much larger than that in thermal equilibrium, significantly overestimating the true equilibrium $L_{\alpha\alpha'}$ necessary for linear response theory. Furthermore, $L_{\alpha\alpha'}^{(1)}$ is inherently size-dependent, while $L_{\alpha\alpha'} = nL_{\alpha\alpha'}^{(1)}$ is intensive, where n is the equilibrium number of defects in the box. Therefore, understanding PD concentration at equilibrium is necessary to accurately model non-equilibrium transport in concentrated solid solutions.

Modern models for PD concentration focus on calculating the distribution of PD formation energies by creating a reference configuration and many defective configurations. In the case of thermal vacancies, these defective configurations are created by removing each atom at each lattice site and calculating their energy differences with the reference configuration using *ab initio* techniques^{[16][17][18][19][20]}. In essence, at each site σ , there's an occupying type $t(\sigma)$, and one considers the two-state system:

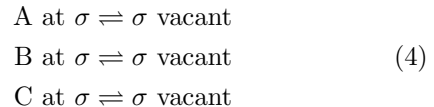
$$t(\sigma) \text{ at } \sigma \rightleftharpoons \sigma \text{ vacant} \quad (3)$$

calculating an effective vacancy formation energy from the resulting statistics over $\{\sigma\}$ with a mean-field-theory approach, treating each site as an independent two-state system. However, for a system that can exchange particles with a reservoir, any finite temperature introduces local fluctuations in composition (A.1), making any choice of a reference configuration ambiguous. For a truly random alloy, this effect is especially relevant, since the presence of a particular atomic type at a lattice site is statistically independent of the atomic types at neighboring sites.

In an approximately random alloy, some chemical ordering will be present, but differing atom types have

comparable occupation probabilities at a given site, including PDs. As such, we argue that one must also include *all* possible occupying types within a mean-field-theory approach, treating each site as an independent $(k+1)$ -state system, where k is the number of alloying elements.

In this work, we present such a mean-field approach using a Langmuir-like model for competitive occupation at individual lattice sites $\{\sigma\}$. For example, in the case of vacancies in an ABC alloy, we consider the competition between the following processes:



similarly calculating vacancy formation quantities from the resulting statistics over $\{\sigma\}$ with a mean-field-theory approach. We then use this model to predict the temperature-dependent vacancy concentration, formation energy, and formation volume for the equiatomic CoNiCrFeMn alloy. To better understand the effects of chemical ordering on vacancy thermodynamics, we additionally perform the same analysis for the equiatomic FeAl alloy because of its tendency to form ordered intermetallic phases^[21].

2 Model

2.1 Substitutional atomic impurity

Consider a lattice with N sites, with each site indexed by σ . In this lattice, the set of possible occupying types is \mathcal{A} , and the well-equilibrated configuration has N_α number of α atoms for all $\alpha \in \mathcal{A}$, and each occupying type of this configuration is denoted by $t(\sigma)$.

Couple the lattice with an energy, volume, and atom-exchanging reservoir with types $\mathcal{A}_r = \mathcal{A} \cup \{\iota\}$, where ι is an impurity type. The reservoir controls the chemical potential, pressure, and temperature of the lattice, thus the probability that a site σ is occupied by ι follows the completely open (constant chemical potential, pressure, and temperature) ensemble^[22]¹:

¹Without a controlled extensive variable, the completely open ensemble is poorly defined for a large system. However, similar to the standard Langmuir adsorption model, the controlled variable is the number of occupiable sites N , which is extensive^[23].

$$\pi_\sigma(\beta) = \frac{1}{Z_\sigma} e^{-\beta(\varepsilon_\sigma + pv_\sigma - \sum_\alpha \mu_\alpha N_\alpha + \mu_{t(\sigma)} - \mu_\iota)} \quad (5)$$

where β and p are respectively $1/k_B T$ and pressure of the reservoir, ε_σ is the energy of the lattice with the impurity occupying σ , v_σ is the relaxed volume of the impurity occupation, μ_α is the chemical potential of α , and Z_σ is the local completely open partition function:

$$Z_\sigma = e^{-\beta(\varepsilon_\sigma + pv_\sigma - \sum_\alpha \mu_\alpha N_\alpha + \mu_{t(\sigma)} - \mu_\iota)} + \sum_{\alpha'} e^{-\beta(E_\sigma^{(\alpha')} + pV_\sigma^{(\alpha')} - \sum_\alpha \mu_\alpha N_\alpha + \mu_{t(\sigma)} - \mu_{\alpha'})} \quad (6)$$

which counts the possible microstates of site σ , which is occupied by all $\alpha \in \mathcal{A}_r$. Essentially, we let all species in \mathcal{A}_r competitively bind onto site σ . Therefore:

$$\pi_\sigma(\beta) = \frac{1}{1 + \sum_\alpha e^{\beta \mathcal{H}_\sigma^{(\alpha)}}} \quad (7)$$

where $\mathcal{H}_\sigma^{(\alpha)} = \varepsilon_\sigma - E_\sigma^{(\alpha)} + p(v_\sigma - V_\sigma^{(\alpha)}) + \mu_\alpha - \mu_\iota$ is the effective enthalpic penalty of swapping an α atom with the impurity ι at site σ . Then, the concentration of ι is the average ι -occupation probability over sites $\{\sigma\}$:

$$x_\iota(\beta) = \langle \pi_\sigma(\beta) \rangle \quad (8)$$

Note that this model is mostly independent of the chosen thermodynamic ensemble, and one can easily choose a different ensemble to evaluate impurity concentration under different conditions. For example, at constant temperature, volume, and chemical potential, we instead have:

$$\mathcal{H}_\sigma^{(\alpha)} = \varepsilon_\sigma - E_\sigma^{(\alpha)} + \mu_\alpha - \mu_\iota \quad (9)$$

Or, at constant temperature, volume, chemical potential, and magnetic field \mathbf{B} :

$$\mathcal{H}_\sigma^{(\alpha)} = \varepsilon_\sigma - E_\sigma^{(\alpha)} - \mathbf{B} \cdot (\mathbf{m}_\sigma - \mathbf{M}_\sigma^{(\alpha)}) + \mu_\alpha - \mu_\iota \quad (10)$$

where \mathbf{m}_σ is the magnetic moment of the lattice with ι occupying site σ and $\mathbf{M}_\sigma^{(\alpha)}$ is the magnetic moment of the lattice with α occupying site σ . Without much loss of generality, we will use the completely open ensemble for the remainder of the calculations. However, we emphasize that the model can be quickly adapted for different ensembles.

2.2 Vacancy impurity

There is no need to perform a lattice-reservoir swap to create a vacancy. All that is necessary is the evaporation of an α atom when creating a vacancy from an α atom at σ . Therefore:

$$\mathcal{H}_\sigma^{(\alpha)} = \varepsilon_\sigma - E_\sigma^{(\alpha)} + p(v_\sigma - V_\sigma^{(\alpha)}) + \mu_\alpha \quad (11)$$

Or, effectively, $\mu_\iota = 0$ if ι is a vacancy, equivalently setting the reference chemical potential to μ_ι .

2.3 Small interstitial impurity

Small interstitials will occupy interstitial sites rather than lattice sites, so we instead track the probability that an interstitial site σ is occupied by a small atom type ι from a set of atom types \mathcal{I} . The probability that a small impurity $\iota \in \mathcal{I}$ occupies a site σ is then:

$$\begin{aligned} \pi_\sigma^{(\iota)}(\beta) &= \frac{e^{-\beta(E_\sigma^{(\iota)} + pV_\sigma^{(\iota)} - \mu_\iota)}}{e^{-\beta(E^\circ + pV^\circ)} + \sum_{\iota'} e^{-\beta(E_\sigma^{(\iota')} + pV_\sigma^{(\iota')} - \mu_{\iota'})}} \\ &= \frac{1}{e^{\beta \mathcal{H}_\sigma^{(\iota)}} + \sum_{\iota'} e^{\beta \mathcal{H}_\sigma^{(\iota, \iota')}}} \end{aligned} \quad (12)$$

where we have two enthalpic penalties, one for placing an impurity of type ι at interstitial site σ :

$$\mathcal{H}_\sigma^{(\iota)} = E_\sigma^{(\iota)} - E^\circ + p(V_\sigma^{(\iota)} - V^\circ) - \mu_\iota \quad (13)$$

and one for swapping an impurity of type ι' with an impurity of type ι at interstitial site σ :

$$\mathcal{H}_\sigma^{(\iota, \iota')} = E_\sigma^{(\iota)} - E_\sigma^{(\iota')} + p(V_\sigma^{(\iota)} - V_\sigma^{(\iota')}) - (\mu_\iota - \mu_{\iota'}) \quad (14)$$

where $E_\sigma^{(\iota)}$ and $V_\sigma^{(\iota)}$ are respectively the relaxed energy and volume of the lattice with an impurity ι at

interstitial site σ , and E° and V° are respectively the relaxed energy and volume of the lattice without impurities.

Here, we count $|\mathcal{I}|+1$ states per site σ , where $|\mathcal{I}|$ is the number of possible occupying impurities, assuming that the larger \mathcal{A} atoms are not stable at interstitial sites. Then, the fraction of interstitial sites occupied by ι is $x_\iota(\beta) = \langle \pi_\sigma^{(\iota)}(\beta) \rangle$.

2.4 Large interstitial impurity

Large interstitial impurities will occupy lattice sites. However, in principle, each α - α' dumbbell interstitial will have a set of metastable directions. Therefore, one must count all single-atom occupation microstates, as well as all α - α' pairs and their associated valid directions.

Due to the larger variety of microstates, this analysis is not trivial, and is thus saved for a future work.

3 Limits

In the dilute limit, the expressions for substitutional impurities (atomic and vacancy) are reduced to:

$$\pi_\sigma(\beta) \approx \frac{1}{\sum_\alpha e^{\beta\mathcal{H}_\sigma^{(\alpha)}}} \quad (15)$$

and the expression for small impurities can be rewritten as:

$$\pi_\sigma^{(\iota)}(\beta) = \frac{1}{\sum_\gamma e^{\beta\mathcal{H}_\sigma^{(\gamma)}}} \quad (16)$$

where $\gamma \in \{\iota\} \cup \{(\iota, \iota') \mid \iota \in \mathcal{I}\}$. As such, we can analyze the same expression for both substitutional and small interstitial impurities by replacing the summation. Therefore, we can sum over \mathcal{A} without loss of generality.

3.1 Homogeneous Limit

For a homogeneous medium with one possible impurity type, we have a unique enthalpic penalty $\mathcal{H} = \mathcal{H}_\sigma^{(\alpha)}$, so $\pi_\sigma(\beta) = x_\iota(\beta)$ for all sites σ . Therefore:

$$x_\iota(\beta) = \frac{1}{e^{\beta\mathcal{H}}} = e^{-\beta\mathcal{H}} \quad (17)$$

recovering the standard Arrhenius expression for impurity concentration.

3.2 High Temperature Limit

In the dilute limit:

$$\ln \pi_\sigma(\beta) = -\ln \left(\sum_\alpha e^{\beta\mathcal{H}_\sigma^{(\alpha)}} \right) \quad (18)$$

Defining a random variable $\mathcal{H}_\sigma^{(\mathcal{A})}$ by a uniform distribution over $\{\mathcal{H}_\sigma^{(\alpha)} \mid \alpha \in \mathcal{A}\}$ yields:

$$\ln \pi_\sigma(\beta) = \ln \frac{1}{|\mathcal{A}|} - \ln \mathbb{E} \left[e^{\beta\mathcal{H}_\sigma^{(\mathcal{A})}} \right] \quad (19)$$

Then $\ln \mathbb{E} \left[e^{\beta\mathcal{H}_\sigma^{(\mathcal{A})}} \right]$ is a cumulant generating function (CGF) of the random variable $\mathcal{H}_\sigma^{(\mathcal{A})}$ (assuming the random variable is temperature-independent), and can thus be expanded in powers of β with cumulants $\kappa_\sigma^{(\ell)}$ as coefficients to some finite order n ^[24]:

$$\pi_\sigma^{(n)}(\beta) = \frac{1}{|\mathcal{A}|} \exp \left(-\sum_{\ell=1}^n \frac{\kappa_\sigma^{(\ell)}}{\ell!} \beta^\ell \right) \quad (20)$$

where $\pi_\sigma^{(n)}(\beta) \rightarrow \pi_\sigma(\beta)$. Then:

$$x_\iota^{(n)}(\beta) = \frac{1}{|\mathcal{A}|} \left\langle \exp \left(-\sum_{\ell=1}^n \frac{\kappa_\sigma^{(\ell)}}{\ell!} \beta^\ell \right) \right\rangle \quad (21)$$

where $x_\iota^{(n)}(\beta) \rightarrow x_\iota(\beta)$. Define the n -dimensional random variable \mathbf{k}_σ as:

$$\mathbf{k}_\sigma = - \left(\kappa_\sigma^{(1)}, \frac{\kappa_\sigma^{(2)}}{2}, \dots, \frac{\kappa_\sigma^{(n)}}{n!} \right) \quad (22)$$

and the variable $\mathbf{b}(\beta)$ as:

$$\mathbf{b} = (\beta, \beta^2, \dots, \beta^n) \quad (23)$$

Therefore:

$$\ln x_\iota^{(n)}(\beta) = \ln \frac{1}{|\mathcal{A}|} + \ln \left\langle e^{\mathbf{b}(\beta) \cdot \mathbf{k}_\sigma} \right\rangle \quad (24)$$

where $\ln \langle e^{\mathbf{b}(\beta) \cdot \mathbf{k}_\sigma} \rangle$ is another CGF. Expanding this CGF about $\mathbf{b}(\beta) = \mathbf{0}$ gives:

$$\begin{aligned} \ln x_i^{(n)}(\beta) &= \ln \frac{1}{|\mathcal{A}|} + \langle \mathbf{k}_\sigma \rangle \cdot \mathbf{b}(\beta) \\ &+ \frac{1}{2} \mathbf{b}(\beta) \cdot \mathbf{K} \mathbf{b}(\beta) + \dots \end{aligned} \quad (25)$$

where \mathbf{K} is the covariance matrix with elements $K_{\ell\ell'}$:

$$K_{\ell\ell'} = \frac{1}{\ell! \ell'!} \left\langle \left(\kappa_\sigma^{(\ell)} - \langle \kappa_\sigma^{(\ell)} \rangle \right) \left(\kappa_\sigma^{(\ell')} - \langle \kappa_\sigma^{(\ell')} \rangle \right) \right\rangle \quad (26)$$

Therefore:

$$x_i^{(n)}(\beta) = \frac{1}{|\mathcal{A}|} e^{-\beta \langle \kappa_\sigma^{(1)} \rangle - \frac{1}{2} \beta^2 (\langle \kappa_\sigma^{(2)} \rangle - K_{11}) + \mathcal{O}(\beta^3)} \quad (27)$$

So, in the high-temperature limit, we recover an Arrhenius expression with activation energy $\langle \frac{1}{|\mathcal{A}|} \sum_\alpha \mathcal{H}_\sigma^{(\alpha)} \rangle$.

4 Methods

To evaluate the concentration of an impurity in a model concentrated alloy, we chose vacancies in equiatomic, face-centered cubic (fcc) Cantor and body-centered cubic (bcc) FeAl alloys, performing atomistic calculations using Large-scale Atomic/Molecular Massively Parallel Simulator (LAMMPS)^{[25][26]}. For the Cantor alloy, we use a modified embedded-atom method^[27] (MEAM) potential developed by Choi et al. to study the effects of individual elements on solid solution hardening^[28]. For FeAl, we use a MEAM potential developed by Lee and Lee to study defect formation behavior^[29].

4.1 Equilibration

Using LAMMPS, we first initialize a random $7 \times 7 \times 7$ fcc Cantor alloy with lattice parameter 3 \AA and minimize the configuration at 0 bar^[30]. Then, we perform an NPT equilibration at 600 K and 1 bar for 10^4 steps with a femtosecond timestep using an integration scheme proposed by Shinoda et al.^[31] with a temperature dampening time of 0.1 ps and a pressure dampening time of 1.0 ps. Lastly, we run a hybrid canonical Monte Carlo/NPT molecular dynamics (MC-MD) routine, where we attempt five α - α'

swaps per α - α' pair every 10^3 MD steps for 10^6 total steps at 600 K, accepting or rejecting each swap with the Metropolis criterion^[32] using the MC package in LAMMPS^[33].

We perform a similar procedure for FeAl, instead starting with a segregated $8 \times 8 \times 8$ body-centered cubic (bcc) solution, and attempting 25 α - α' swaps every 10^3 steps. (Figure 1)

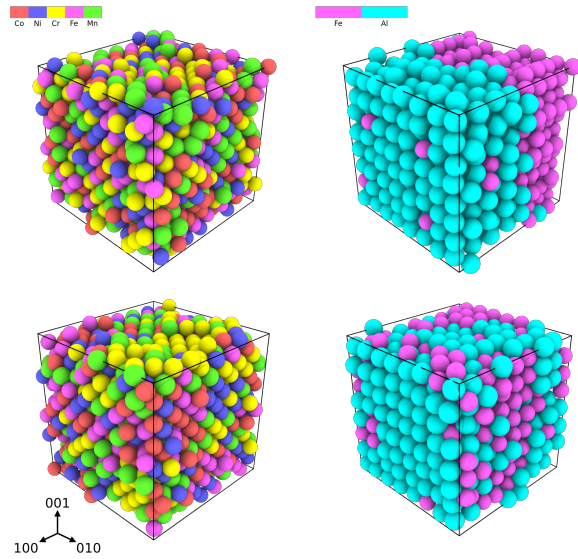


Figure 1: MC-MD snapshots of the Cantor (left) and FeAl (right) systems at 0 ns (top) and 1 ns (bottom) rendered with OVITO^[34].

To quantify the equilibration, we first calculated the Cowley short-range order (SRO) parameter^[35] for each α - α' type pair:

$$\chi_{\alpha\alpha'} = 1 - \frac{p_{\alpha\alpha'}}{(2 - \delta_{\alpha\alpha'})x_\alpha x_{\alpha'}} \quad (28)$$

where $p_{\alpha\alpha'}$ is the probability of finding types α and α' in the first nearest-neighbor shell. Due to the similarity of the nearest-neighbor and next-nearest-neighbor distances in bcc structures, we first apply a score-based denoising algorithm proposed by Hsu et al.^[36] before calculating the SRO parameters.

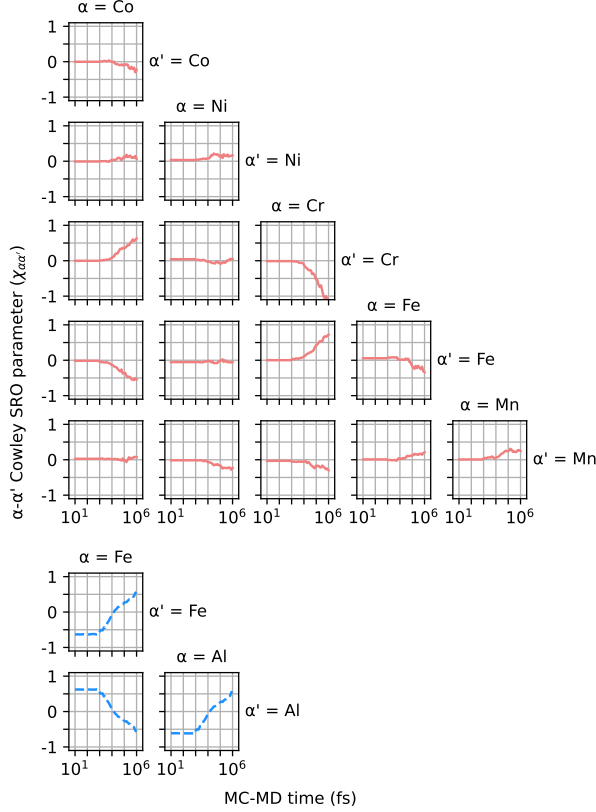


Figure 2: Cowley SRO parameters $\chi_{\alpha\alpha'}$ as a function of MC-MD simulation time for the Cantor alloy (top) and FeAl (bottom) after score-based denoising.

Note that the MC-MD steps are sampled at a logarithmic frequency (50 steps between 10 fs and 1 ns) in order to obtain high resolution information over the fast initial equilibration steps.

Although Eq. (28) differs from the traditional expression for the Cowley SRO parameters, which uses a conditional probability as opposed to an unconditional probability, Rao and Curtin proved that they are equivalent^[37]. The $\chi_{\alpha\alpha'}$ calculations are implemented as an OVITO modifier in a lightweight library available in the Python Package Index^[38].

4.2 Energetics Calculation

After equilibrating with MC-MD, the resulting configuration is relaxed at 0 bar.

Then, we select the site $\sigma = 1$ (starting site indexing at 1), inserting all types $\alpha \in \mathcal{A}$ and again minimizing at 0 bar, calculating the resulting interaction energy $E_{\sigma}^{(\alpha)}$ and volume $V_{\sigma}^{(\alpha)}$. For the same lattice site, we

then remove the current occupying atom, one again minimizing at 0 bar and calculating the resulting interaction energy ε_{σ} and volume v_{σ} .

Then, we iterate to the next site $\sigma \leftarrow \sigma + 1$, loading in the aforementioned 0 bar configuration, and repeating the aforementioned energetics/volumetrics calculations, storing all values $E_{\sigma}^{(\alpha)}$, $V_{\sigma}^{(\alpha)}$, ε_{σ} , and v_{σ} for post-processing.

4.3 Chemical Potential Calculation

After adding an atom of type α to a system with free energy G° , the new free energy is:

$$G_{\alpha} = G^{\circ} + \mu_{\alpha} \quad (29)$$

Therefore, swapping an α atom with an α' atom results in a free energy change equal to their respective chemical potential differences:

$$G_{\alpha} - G_{\alpha'} = \mu_{\alpha} - \mu_{\alpha'} \quad (30)$$

As an approximation, we evaluate free energy differences at 0 K and 0 bar for each α - α' pair, where free energy is equal to internal energy:

$$\langle E_{\sigma}^{(\alpha)} - E_{\sigma}^{(\alpha')} \rangle = \mu_{\alpha} - \mu_{\alpha'} \quad (31)$$

Additionally, using the Euler equation for enthalpy at 0 K yields:

$$h = \sum_{\alpha} x_{\alpha} \mu_{\alpha} \quad (32)$$

where h is the enthalpy per atom of the well-equilibrated crystal. For a k -component system, we can generate $m = \frac{1}{2}k(k-1)$ equations from (31) (one per (α, α') pair), plus (32), which is an overdetermined system for $k > 2$, defined by:

$$A\boldsymbol{\mu} = \boldsymbol{\Delta} \quad (33)$$

where, if each (α, α') pair is indexed by $0 \leq i \leq m$, then the elements of A , $\boldsymbol{\mu}$, and $\boldsymbol{\Delta}$ are defined by:

$$\begin{aligned}
A_{i\alpha} &= 1 \\
A_{i\alpha'} &= -1 \\
A_{m\alpha} &= x_\alpha \\
\Delta_i &= \left\langle E_\sigma^{(\alpha)} - E_\sigma^{(\alpha')} \right\rangle \\
\Delta_m &= h \\
\mu_\alpha &= \mu_\alpha
\end{aligned} \tag{34}$$

α	Co	Ni	Cr	Fe	Mn
μ_α	-4.48	-4.57	-3.95	-4.28	-3.09

α	Fe	Al
μ_α	-4.62	-3.50

Table 1: Chemical potentials (in eV) calculated from (33) and (34) at the final MC-MD snapshot for the CoNiCrFeMn (top) and FeAl (bottom) systems.

Equation (32) defines the reference chemical potential in terms of the zero-point energy, while (31) defines the chemical potential differences between each atom type.

Note that (31) closely resembles the Widom insertion method^[39]. The traditional implementation of this method, where single particles are removed, would skew our chemical potential calculations since the removal of an atom would introduce a high-energy vacancy. Removing a particle and then adding a new particle avoids this bias.

Instead of relying on a 0K and 0bar approximation for use in (30), one can also calculate free energy at a given temperature and pressure using thermodynamic integration methods (such as adiabatic switching^{[40][41]}, finite difference thermodynamic integration^[42], Bennet’s acceptance ratio method^[43], etc.).

5 Results

5.1 Formation Quantities

Expanding about $\beta = \beta^\circ$ and $p = p^\circ$ to first order in β and p gives:

$$\begin{aligned}
\ln x_V(\beta, p) &= \ln x_V(\beta^\circ, p^\circ) - \beta E_{\text{form}}(\beta^\circ, p^\circ) \\
&\quad - \beta^\circ p \Omega_{\text{form}}(\beta^\circ, p^\circ)
\end{aligned} \tag{35}$$

where $E_{\text{form}}(\beta^\circ, p^\circ)$ and $\Omega_{\text{form}}(\beta^\circ, p^\circ)$ are respectively the formation energy and formation volume at $(\beta, p) = (\beta^\circ, p^\circ)$. Therefore:

$$\begin{aligned}
E_{\text{form}}(\beta, p) &= - \left(\frac{\partial \ln x_V(\beta, p)}{\partial \beta} \right)_p \\
&= \frac{1}{x_V(\beta)} \left\langle \frac{\sum_\alpha (\varepsilon_\sigma - \mathcal{H}_\sigma^{(\alpha)}) e^{\beta \mathcal{H}_\sigma^{(\alpha)}}}{\left(1 + \sum_\alpha e^{\beta \mathcal{H}_\sigma^{(\alpha)}}\right)^2} \right\rangle
\end{aligned} \tag{36}$$

and:

$$\begin{aligned}
\Omega_{\text{form}}(\beta, p) &= - \left(\frac{\partial \ln x_V(\beta, p)}{\partial(\beta p)} \right)_\beta \\
&= \frac{1}{x_V(\beta)} \left\langle \frac{\sum_\alpha (v_\sigma - V_\sigma^{(\alpha)}) e^{\beta \mathcal{H}_\sigma^{(\alpha)}}}{\left(1 + \sum_\alpha e^{\beta \mathcal{H}_\sigma^{(\alpha)}}\right)^2} \right\rangle
\end{aligned} \tag{37}$$

Using our site statistics and the chemical potentials calculated from (33) and (34), we can calculate all $\mathcal{H}_\sigma^{(\alpha)}$ ’s from (11).

Notably, both formation quantities respectively depend on statistics of enthalpic and volumetric differences between vacant states and α -occupying states. Statistics for these quantities for the final MC-MD snapshot are shown in Figure 3.

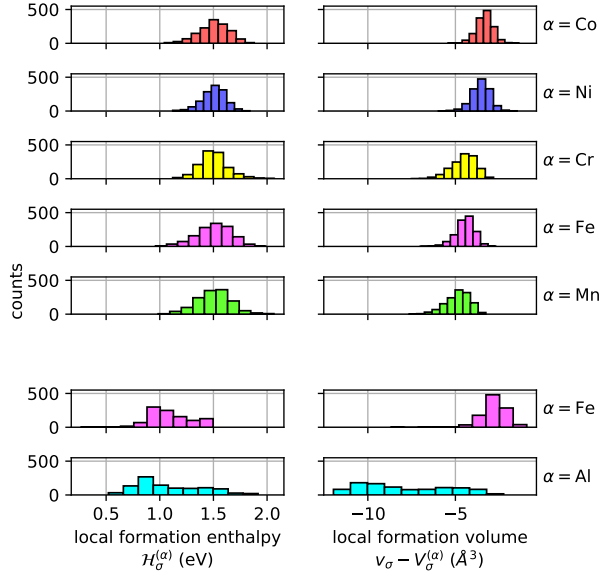


Figure 3: Histograms of local enthalpic and volumetric penalties, respectively $\mathcal{H}_\sigma^{(\alpha)}$ and $v_\sigma - V_\sigma^{(\alpha)}$, at the final MC-MD snapshot for the Cantor (top) and FeAl (bottom) systems.

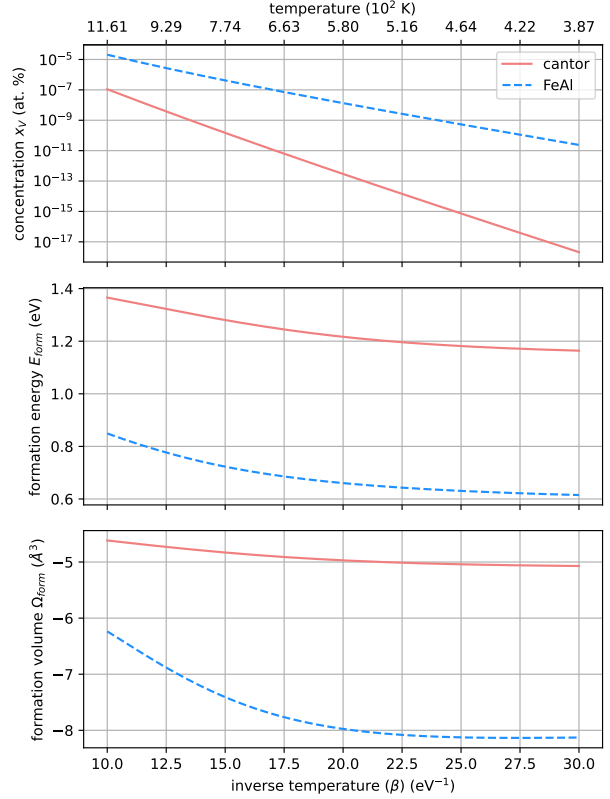


Figure 4: Vacancy concentration (top), formation energy (middle), and formation volume (bottom) as a function of temperature at the final MC-MD snapshot.

Note the strong temperature dependence on the formation energy and formation volume. Both formation energy and volume monotonically increase with temperature, with formation energy notably changing more than 0.2 eV over the 387 K-1161 K range for both alloy systems.

More generally, we can calculate any vacancy formation quantity ξ_{form} conjugate to some external generalized force X (for example, an external magnetic field) by defining said formation quantity via an expansion about $(\beta, p, X) = (\beta^\circ, p^\circ, X^\circ)$:

$$\begin{aligned}
 \ln x_V(\beta, p, X) = & \ln x_V(\beta^\circ, p^\circ, X^\circ) \\
 & - \beta E_{\text{form}}(\beta^\circ, p^\circ, X^\circ) \\
 & - \beta^\circ p \Omega_{\text{form}}(\beta^\circ, p^\circ, X^\circ) \\
 & + \beta^\circ X \xi_{\text{form}}(\beta^\circ, p^\circ, X^\circ)
 \end{aligned} \tag{38}$$

From these statistics, we can calculate $x_V(\beta)$, $E_{\text{form}}(\beta)$, and $\Omega_{\text{form}}(\beta)$ for the final MC-MD snapshot. Note that we implicitly set $p = 0$.

which then implies:

$$\begin{aligned} \xi_{\text{form}}(\beta, p, X) &= \left(\frac{\partial \ln x_V(\beta, p, X)}{\partial(\beta X)} \right)_{\beta, p} \\ &= -\frac{1}{x_V(\beta)} \left\langle \frac{\sum_{\alpha} \left(\xi_{\sigma} - \Xi_{\sigma}^{(\alpha)} \right) e^{\beta \mathcal{H}_{\sigma}^{(\alpha)}}}{\left(1 + \sum_{\alpha} e^{\beta \mathcal{H}_{\sigma}^{(\alpha)}} \right)^2} \right\rangle \end{aligned} \quad (39)$$

where ξ_{σ} is the generalized displacement of the impurity occupying site σ , and $\Xi_{\sigma}^{(\alpha)}$ is the generalized displacement of an α atom occupying site σ .

5.2 Vacancies and Order

At each step that we compute $\chi_{\alpha\alpha'}$, we perform the vacancy insertions and their associated thermodynamic calculations to calculate vacancy concentration, formation energy, and formation volume for configurations with different ordering (Figure 5).

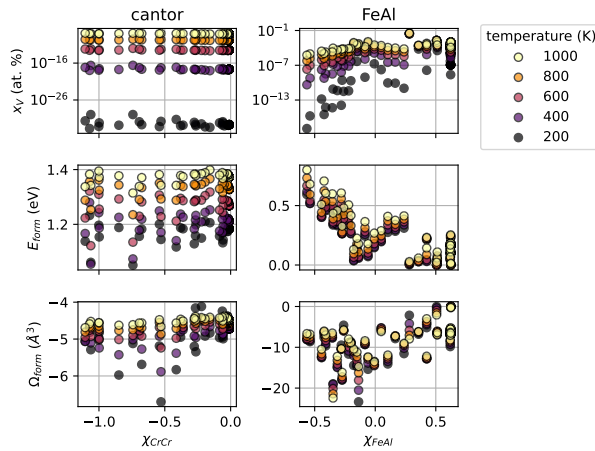


Figure 5: Vacancy concentration (top), formation energy (middle), and formation volume (bottom) as a function of an ordering parameter for various temperatures for the Cantor (left) and FeAl (right) systems.

For the Cantor alloy, there is not a clear correlation between χ_{CrCr} and vacancy concentration, formation energy, nor formation volume at any tested temperature. However, for FeAl, vacancy concentration and formation volume increase with χ_{FeAl} , while formation energy decreases with χ_{FeAl} (Figure 5), with the trend between chemical ordering and vacancy concentration becoming flatter at high temperatures. In particular, vacancy concentration and formation energy reach extreme values (high concentration and small formation energy) for high χ_{FeAl} . Note that the

high χ_{FeAl} configurations, where Fe and Al are phase-separated, are very far out-of-equilibrium, leading to high-energy occupied states, and thus having similar energetics between vacant and occupied states. In comparison, the Cantor system is closer to equilibrium over the range of sampled ordering parameters, yielding a large energetic difference between vacant and occupied states.

6 Limitations

Our methodology does not account for binding between impurities. While it should remain true that each site's occupation numbers follow the completely open ensemble and that the concentration of the impurity is the thermodynamic average of the impurity's occupation probability, we take a naive averaging procedure that does not account for correlations between sites, which can be problematic for many relevant solid solutions, such as those with a large number of divacancies, voids, and/or dislocations. Another example would be He in stainless steel, where He tends to precipitate^[44]. Even without a high tendency to bind, correlations between impurity occupation probabilities will be relevant outside of the dilute limit. However, the dilute limit is usually well-respected below the melting point^{[45][46]}.

Furthermore, sampling with a single well-equilibrated configuration might not be sufficient for small systems. For a full analysis, one should not only swap atom types at single sites, but also analyze all possible environments around those single sites. This is problematic for an *ab initio* technique that introduces size constraints.

We also implicitly assume that energetics are independent of temperature. However, it has been predicted that local quasi-harmonicity and anharmonicity both play a crucial role in vacancy formation thermodynamics in Al and Cu^[47]. Therefore, it might not be sufficient to only count microstates at 0 K.

Lastly, the Cantor interatomic potential used in this work was not fitted to vacancy energetics. As such, we expect a limited ability of quantitative prediction of our model using this potential. However, any energy-calculating method can be used to get the necessary data to predict impurity concentration. Using the MolSSI Driver Interface library^[48], one can couple an *ab initio* method to LAMMPS for easy reuse of our prewritten input files and data analysis scripts.

7 Conclusions

In summary, we introduce a flexible single-site Langmuir model for competitive impurity occupation and use this model to predict impurity concentration in any concentrated solid solution, including vacancies, small interstitial, and large interstitial impurities. This model can be modified to incorporate any thermodynamic ensemble, allowing for the prediction of impurity thermodynamics as a function of various thermodynamic forces. We then analyze the limits of this model, calculating an effective formation energy in the high-temperature limit.

We then use this model to predict the vacancy concentration, formation energy, and formation volume of the Cantor and FeAl alloys at 0 bar, and calculate all of these quantities as a function of short-range order, annealing from a random solution for the Cantor alloy and a segregated solution for FeAl. We show that, for the Cantor system over the 200 K to 1000 K range, there is no clear correlation between short-range order and vacancy thermodynamics. For the FeAl system over the same temperature range, however, vacancy thermodynamics strongly depend on short-range order. We provide code and a corresponding tutorial to analyze and reproduce our results using LAMMPS, allowing for the quick evaluation of our model for a different use case.

8 Data Availability

All data, LAMMPS input files, post-processing scripts, and a brief tutorial for using the files and scripts are available on GitHub^{[49][50][51]}.

9 Acknowledgements

Authors acknowledge support from the U.S. Department of Energy, Office of Basic Energy Sciences, Materials Science and Engineering Division under Award No. DE-SC0022980.

Additionally, this material is based on work supported by the National Science Foundation under Grant Nos. MRI# 2024205, MRI# 1725573, and CRI# 2010270 for allotment of compute time on the Clemson University Palmetto Cluster.

10 Disclaimer

Any opinions, findings, and conclusions or recommendations expressed in this material are those of the author(s) and do not necessarily reflect the views of the National Science Foundation.

A Appendix

A.1 Local composition fluctuations in grand canonical ensemble

Here we model our single site that can be occupied by \mathcal{A} atom types. The grand canonical partition function \mathcal{Z} is the discrete Laplace transform of the canonical partition function Z :

$$\mathcal{Z}(\beta, \boldsymbol{\mu}) = \sum_{\mathbf{n}} e^{\beta \boldsymbol{\mu}^T \mathbf{n}} Z(\beta, \mathbf{n}) \quad (40)$$

where $\boldsymbol{\mu}$ is a vector holding all chemical potentials (μ_1, \dots) for all $\alpha \in \mathcal{A}$ and \mathbf{n} is an occupation vector where $n_\alpha = 1$ if α occupies the site. Since only one atom type can occupy the site at once:

$$\mathcal{Z}(\beta, \boldsymbol{\mu}) = \frac{1}{2} \sum_{\alpha} \lambda_{\alpha} \operatorname{csch} \frac{\beta \varepsilon_{\alpha}}{2} \quad (41)$$

where each particle is modeled as a quantum harmonic oscillator with frequency $\varepsilon_{\alpha}/\hbar$ and $\lambda_{\alpha} = e^{\beta \mu_{\alpha}}$ is the fugacity of α . Then:

$$\begin{aligned} \langle \mathbf{n} \rangle &= \frac{\sum_{\mathbf{n}} \mathbf{n} e^{\beta \boldsymbol{\mu}^T \mathbf{n}} Z(\beta, \mathbf{n})}{\sum_{\mathbf{n}} e^{\beta \boldsymbol{\mu}^T \mathbf{n}} Z(\beta, \mathbf{n})} \\ &= (\nabla_{\beta \boldsymbol{\mu}} \ln \mathcal{Z})_{\beta} \end{aligned} \quad (42)$$

$$\langle \mathbf{n} \cdot \mathbf{n} \rangle = 1$$

Therefore, the fluctuation in occupancy is:

$$\begin{aligned} \Delta n &= \sqrt{\langle \mathbf{n} \cdot \mathbf{n} \rangle - \langle \mathbf{n} \rangle \cdot \langle \mathbf{n} \rangle} \\ &= \sqrt{1 - \sum_{\alpha} \left(\left(\frac{\partial \ln \mathcal{Z}}{\partial (\beta \mu_{\alpha})} \right)_{\beta, \{\mu_{\alpha'} | \alpha' \neq \alpha\}} \right)^2} \\ &= \sqrt{1 - \frac{\sum_{\alpha} \left(\lambda_{\alpha} \operatorname{csch} \frac{\beta \varepsilon_{\alpha}}{2} \right)^2}{\left(\sum_{\alpha} \lambda_{\alpha} \operatorname{csch} \frac{\beta \varepsilon_{\alpha}}{2} \right)^2}} \end{aligned} \quad (43)$$

Assuming each atom type has the same vibrational frequency, then:

$$\Delta n = \sqrt{1 - \frac{\sum_{\alpha} \lambda_{\alpha}^2}{(\sum_{\alpha} \lambda_{\alpha})^2}} \quad (44)$$

which is plotted for our calculated chemical potentials in Table 1.

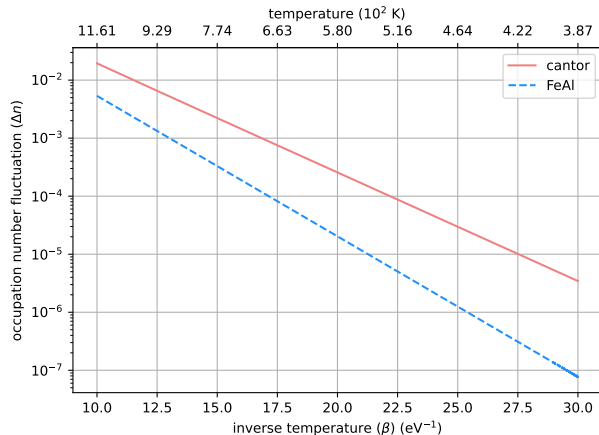


Figure 6: Δn as a function of temperature using chemical potentials from Table 1.

References

- [1] F. Otto, A. Dlouhý, Ch. Somsen, H. Bei, G. Eggeler, and E.P. George. The influences of temperature and microstructure on the tensile properties of a CoCrFeMnNi high-entropy alloy. *Acta Materialia*, 61(15):5743–5755, 2013.
- [2] Zhouan Zhang, David E.J. Armstrong, and Patrick S. Grant. The effects of irradiation on CrMnFeCoNi high-entropy alloy and its derivatives. *Progress in Materials Science*, 123:100807, 2022. A Festschrift in Honor of Brian Cantor.
- [3] F. Otto, A. Dlouhý, K.G. Pradeep, M. Kuběnová, D. Raabe, G. Eggeler, and E.P. George. Decomposition of the single-phase high-entropy alloy CrMnFeCoNi after prolonged anneals at intermediate temperatures. *Acta Materialia*, 112:40–52, 2016.
- [4] Y. J. Li, A. Savan, and A. Ludwig. Atomic scale understanding of phase stability and decomposition of a nanocrystalline CrMnFeCoNi Cantor alloy. *Applied Physics Letters*, 119(20):201910, 11 2021.
- [5] Yukitaka Murakami, Toshihiko Kanazaki, Yoji Mine, and Saburo Matsuoka. Hydrogen embrittlement mechanism in fatigue of austenitic stainless steels. *Metallurgical and Materials Transactions A*, 39(6):1327–1339, Jun 2008.
- [6] Timothy M. Krentz Michael J. Morgan, Dale A. Hitchcock and Scott L. West. Tritium aging effects on fracture toughness of stainless steel weldments. *Fusion Science and Technology*, 76(3):209–214, 2020.
- [7] Terumitsu Miura, Katsuhiko Fujii, and Koji Fukuya. Micro-mechanical investigation for effects of helium on grain boundary fracture of austenitic stainless steel. *Journal of Nuclear Materials*, 457:279–290, 2015.
- [8] B. Radiguet, A. Etienne, P. Pareige, X. Sauvage, and R. Valiev. Irradiation behavior of nanostructured 316 austenitic stainless steel. *Journal of Materials Science*, 43(23):7338–7343, Dec 2008.
- [9] A.R. Allnatt and A.B. Lidiard. *Atomic Transport in Solids*. Cambridge University Press, 2003.
- [10] M. Nastar and F. Soisson. 1.18 - radiation-induced segregation. In Rudy J.M. Konings, editor, *Comprehensive Nuclear Materials*, pages 471–496. Elsevier, Oxford, 2012.
- [11] Alper T. Celebi, Seyed Hossein Jamali, André Bardow, Thijs J. H. Vlugt, and Othonas A. Moulτος. Finite-size effects of diffusion coefficients computed from molecular dynamics: a review of what we have learned so far. *Molecular Simulation*, 47(10-11):831–845, 2021.
- [12] Thomas Garnier and Maylise Nastar. Coarse-grained kinetic Monte Carlo simulation of diffusion in alloys. *Phys. Rev. B*, 88:134207, Oct 2013.
- [13] D. Paschek and R. Krishna. Kinetic Monte Carlo simulations of transport diffusivities of binary mixtures in zeolites. *Phys. Chem. Chem. Phys.*, 3:3185–3191, 2001.
- [14] J.B. Piochaud, M. Nastar, F. Soisson, L. Thuinet, and A. Legris. Atomic-based phase-field method for the modeling of radiation

- induced segregation in Fe–Cr. *Computational Materials Science*, 122:249–262, 2016.
- [15] A R Allnatt. Einstein and linear response formulae for the phenomenological coefficients for isothermal matter transport in solids. *Journal of Physics C: Solid State Physics*, 15(27):5605, sep 1982.
- [16] A. V. Ruban. Thermal vacancies in random alloys in the single-site mean-field approximation. *Phys. Rev. B*, 93:134115, Apr 2016.
- [17] Anus Manzoor, Yongfeng Zhang, and Dilpuneet S. Aidhy. Factors affecting the vacancy formation energy in Fe₇₀Ni₁₀Cr₂₀ random concentrated alloy. *Computational Materials Science*, 198:110669, 2021.
- [18] Weiliang Chen, Xueyong Ding, Yuchao Feng, Xiongjun Liu, Kui Liu, Z.P. Lu, Dianzhong Li, Yiyi Li, C.T. Liu, and Xing-Qiu Chen. Vacancy formation enthalpies of high-entropy FeCoCrNi alloy via first-principles calculations and possible implications to its superior radiation tolerance. *Journal of Materials Science & Technology*, 34(2):355–364, 2018.
- [19] J. B. Piochaud, T. P. C. Klaver, G. Adjanor, P. Olsson, C. Domain, and C. S. Becquart. First-principles study of point defects in an fcc Fe-10Ni-20Cr model alloy. *Phys. Rev. B*, 89:024101, Jan 2014.
- [20] Congyi Li, Junqi Yin, Khorgolkhuu Odbadrakh, Brian C. Sales, Steven J. Zinkle, G. Malcolm Stocks, and Brian D. Wirth. First principle study of magnetism and vacancy energetics in a near equimolar NiFeMnCr high entropy alloy. *Journal of Applied Physics*, 125(15):155103, 04 2019.
- [21] C. G. McKamey. *Iron Aluminides*, pages 351–391. Springer US, Boston, MA, 1996.
- [22] Ugo Marzolino. μPT statistical ensemble: systems with fluctuating energy, particle number, and volume. *Scientific Reports*, 11(1):15096, Jul 2021.
- [23] M. Volmer. Thermodynamische folgerungen ans der zustandsgleichung für adsorbierte stoffe. *Zeitschrift für Physikalische Chemie*, 115U(1):253–260, 1925.
- [24] David R. Brillinger. *Time Series: Data Analysis and Theory*. SIAM: Society for Industrial and Applied Mathematics, 9 2001.
- [25] Aidan P. Thompson, H. Metin Aktulga, Richard Berger, Dan S. Bolintineanu, W. Michael Brown, Paul S. Crozier, Pieter J. in ’t Veld, Axel Kohlmeyer, Stan G. Moore, Trung Dac Nguyen, Ray Shan, Mark J. Stevens, Julien Tranchida, Christian Trott, and Steven J. Plimpton. LAMMPS - a flexible simulation tool for particle-based materials modeling at the atomic, meso, and continuum scales. *Computer Physics Communications*, 271:108171, 2022.
- [26] Large-scale Atomic/Molecular Massively Parallel Simulator. <https://lammps.org/>.
- [27] M. I. Baskes, J. S. Nelson, and A. F. Wright. Semiempirical modified embedded-atom potentials for silicon and germanium. *Phys. Rev. B*, 40:6085–6100, Sep 1989.
- [28] Won-Mi Choi, Yong Hee Jo, Seok Su Sohn, Sunghak Lee, and Byeong-Joo Lee. Understanding the physical metallurgy of the CoCr-FeMnNi high-entropy alloy: an atomistic simulation study. *npj Computational Materials*, 4(1):1, Jan 2018.
- [29] Eunkoo Lee and Byeong-Joo Lee. Modified embedded-atom method interatomic potential for the Fe–Al system. *Journal of Physics: Condensed Matter*, 22(17):175702, apr 2010.
- [30] M. Parrinello and A. Rahman. Polymorphic transitions in single crystals: A new molecular dynamics method. *Journal of Applied Physics*, 52(12):7182–7190, 12 1981.
- [31] Wataru Shinoda, Motoyuki Shiga, and Masuhiro Mikami. Rapid estimation of elastic constants by molecular dynamics simulation under constant stress. *Phys. Rev. B*, 69:134103, Apr 2004.
- [32] Nicholas Metropolis, Arianna W. Rosenbluth, Marshall N. Rosenbluth, Augusta H. Teller, and Edward Teller. Equation of State Calculations by Fast Computing Machines. *The Journal of Chemical Physics*, 21(6):1087–1092, 12 2004.
- [33] Babak Sadigh, Paul Erhart, Alexander Stukowski, Alfredo Caro, Enrique Martinez, and Luis Zepeda-Ruiz. Scalable parallel Monte Carlo algorithm for atomistic simulations of

- precipitation in alloys. *Phys. Rev. B*, 85:184203, May 2012.
- [34] Alexander Stukowski. Visualization and analysis of atomistic simulation data with OVITO—the Open Visualization Tool. *Modelling Simul. Mater. Sci. Eng.*, 18(1), Jan 2010.
- [35] J. M. Cowley. An approximate theory of order in alloys. *Phys. Rev.*, 77:669–675, Mar 1950.
- [36] Tim Hsu, Babak Sadigh, Nicolas Bertin, Cheol Woo Park, James Chapman, Vasily Bulatov, and Fei Zhou. Score-based denoising for atomic structure identification, 2023.
- [37] Y. Rao and W.A. Curtin. Analytical models of short-range order in FCC and BCC alloys. *Acta Materialia*, 226:117621, 2022.
- [38] Jacob Jeffries. cowley-sro-parameters. <https://pypi.org/project/cowley-sro-parameters/>.
- [39] B. Widom. Some Topics in the Theory of Fluids. *The Journal of Chemical Physics*, 39(11):2808–2812, 08 1963.
- [40] M. de Koning and A. Antonelli. Einstein crystal as a reference system in free energy estimation using adiabatic switching. *Phys. Rev. E*, 53:465–474, Jan 1996.
- [41] Rodrigo Freitas, Mark Asta, and Maurice de Koning. Nonequilibrium free-energy calculation of solids using LAMMPS. *Computational Materials Science*, 112:333–341, 2016.
- [42] M. Mezei. The finite difference thermodynamic integration, tested on calculating the hydration free energy difference between acetone and dimethylamine in water. *The Journal of Chemical Physics*, 86(12):7084–7088, 06 1987.
- [43] Charles H Bennett. Efficient estimation of free energy differences from Monte Carlo data. *Journal of Computational Physics*, 22(2):245–268, 1976.
- [44] H. Schroeder J. Rothaut and H. Ullmaier. The growth of helium bubbles in stainless steel at high temperatures. *Philosophical Magazine A*, 47(5):781–795, 1983.
- [45] R.W. Siegel. Vacancy concentrations in metals. *Journal of Nuclear Materials*, 69-70:117–146, 1978.
- [46] Yaakov Kraftmakher. Equilibrium vacancies and thermophysical properties of metals. *Physics Reports*, 299(2):79–188, 1998.
- [47] A. Glensk, B. Grabowski, T. Hickel, and J. Neugebauer. Breakdown of the Arrhenius law in describing vacancy formation energies: The importance of local anharmonicity revealed by ab initio thermodynamics. *Phys. Rev. X*, 4:011018, Feb 2014.
- [48] Taylor A. Barnes, Eliseo Marin-Rimoldi, Samuel Ellis, and T. Daniel Crawford. The MolSSI driver interface project: A framework for standardized, on-the-fly interoperability between computational molecular sciences codes. *Computer Physics Communications*, 261:107688, 2021.
- [49] Jacob Jeffries. jwjeffr/impurities. <https://github.com/jwjeffr/impurities>.
- [50] Charles R. Harris, K. Jarrod Millman, Stéfan J. van der Walt, Ralf Gommers, Pauli Virtanen, David Cournapeau, Eric Wieser, Julian Taylor, Sebastian Berg, Nathaniel J. Smith, Robert Kern, Matti Picus, Stephan Hoyer, Marten H. van Kerkwijk, Matthew Brett, Allan Haldane, Jaime Fernández del Río, Mark Wiebe, Pearu Peterson, Pierre Gérard-Marchant, Kevin Sheppard, Tyler Reddy, Warren Weckesser, Hameer Abbasi, Christoph Gohlke, and Travis E. Oliphant. Array programming with NumPy. *Nature*, 585(7825):357–362, September 2020.
- [51] J. D. Hunter. Matplotlib: A 2D graphics environment. *Computing in Science & Engineering*, 9(3):90–95, 2007.